Systematic Study on Crystal Structure and Properties of $FeSr_2LnCu_2O_{7+\delta}$ (Ln = La, Nd, Sm, Eu, Gd, Dy, Ho, Er, and Yb)

L. T. Yang,*[,†] J. K. Liang,*[,†,‡] Q. L. Liu,[†] H. M. Fan,[†] G. B. Song,[†] X. M. Feng,[†] H. F. Yang,[†] and G. H. Rao[†]

Institute of Physics and Center for Condensed Matter Physics, Chinese Academy of Sciences, P.O. Box 603, Beijing 100080, PR China, and International Center for Materials Physics, Academia Sinica, Shenyang 110016, PR China

Received July 13, 2003. Revised Manuscript Received October 9, 2003

The crystal structures of a series of new compounds with the composition $FeSr_2LnCu_2O_{7+\delta}$ (Ln = La, Nd, Sm, Eu, Gd, Dy, Ho, Er, and Yb) that were successfully synthesized by solid-state reaction are investigated. The Rietveld refinement of the X-ray diffraction data shows that the samples exhibit a transition from a tetragonal system with space group *P*4/*mmm* for light rare earths Ln = La, Nd, Sm, Eu, and Gd to an orthorhombic system with space group *Pmmm* for heavy rare earths Ln = Dy, Ho, Er, and Yb. The oxygen contents of the samples are chemically determined by the iodometric titration. The room-temperature Mössbauer spectroscopy of ^{57}Fe in $FeSr_2GdCu_2O_{7+\delta}$ is used to study the site distribution of Fe between the 1a and 2g sites in the as-synthesized in the air samples and O_2-annealed samples, respectively. In the as-synthesized sample, there are about 67% of Fe ions residing in the 1a site, whereas in the O_2-annealed sample, there are about 61% of Fe ions residing on the 1a site. Magnetization measurements indicate that χ changes with temperature in a Curie-type manner. Resistance measurements indicate that these samples have a semiconductor-like behavior and their band gap is related to their structural type and the radius of rare earth ions.

1. Introduction

The crystal structure, i.e., the arrangement of atoms in a material, largely determines its physical properties. Precise structure determination is then one of the basic requirements for any new substances. This is particularly true for the high-T_c perovskite-type compounds whose superconducting properties are strongly related to their structural details.

Recent discovery of the coexistence of superconductivity (SC) and ferromagnetism (FM) in the ruthenate-cuprate compound $RuSr_2LnCu_2O_{7+\delta}$ with Ln = Gd,Eu[1−8] has attracted widespread interest. The ferromagnetic (FM)-like order appears at Curie temperature of T_M = 130−150 K, whereas superconductivity occurs at a significantly lower superconducting (SC) transition temperature T_c = 15−45 K.[6] They have thus been called FM superconductors. The crystal structure of these compounds is similar to that of $LnBa_2Cu_3O_7$ except for the replacement of Cu in 1a site by Ru atom. Ru and Fe belong to the same group in the periodic table of elements and they exhibit many similar physical and chemical properties. Takashi Mochiku et al.[9] also reported a superconductivity around 50 K in $FeSr_2YCu_2O_{7.68}$ annealed in N_2 atmosphere, and subsequently in a high-pressure O_2 atmosphere. In a high magnetic field the magnetic ordering at low temperature around 20 K was also observed in this compound. In this superconductive phase about 81% Fe atom resided on 1a site and residual Fe was located on 2g site. Comparing with the results of neutron diffraction study of nonsuperconductive sample $FeSr_2YCu_2O_{7.42}$ which was reported by Slater and Greaves,[10] Takashi Mochiku et al.[9] concluded that superconductivity in the sample $FeSr_2YCu_2O_{7.68}$ is caused both by the ordered distribution of Cu and Fe atoms due to the N_2-annealing and by the increase of the oxygen content in a high-pressure O_2. This result suggests us a new way to study these compounds in which the superconductivity has not yet been discovered.

* Corresponding authors. E-mail: ltyang@aphy.iphy.ac.cn; jkliang@aphy.iphy.ac.cn.
† Chinese Academy of Sciences.
‡ Academia Sinica.

(1) Bauernfeind, L.; Widder, W.; Braun, H. F. *Physica C*. **1995**, *254*, 151.
(2) McLaughlin, A. C.; Zhou, W.; Attfield, J. P.; Fitch, A. N.; Tallon, J. L. *Phys. Rev. B* **1999**, *60*, 7512.
(3) Tallon, J. L.; Loram, J. W.; Williams, G. V. M.; Bernhard, C. *Phys. Rev. B* **2000**, *61*, 6471.
(4) Bernhard, C.; Tallon, J. L.; Brücher, E.; Kremer, R. K. *Phys. Rev. B* **2000**, *61*, 14960.
(5) Chu, C. W.; Xue, Y. Y.; Tsui, S.; Cmaidalka, J.; Heilman, A. K.; Lorenz, B.; Meng, R. L. *Physica C* **2000**, *335*, 231.
(6) Bernhard, C.; Tallon, J. L.; Niedermayer, Ch.; Blasius, Th.; Golnik, A.; Brücher E.; Kremer, R. K.; Noakes, D. R.; Stronach, C. E.; Ansaldo, E. J. *Phys. Rev. B* **1999**, *59*, 14099.
(7) Lynn, J. W.; Keimer, B.; Ulrich, C.; Bernhard, C.; Tallon, J. L. *Phys. Rev. B* **2000**, *61*, 14964.
(8) Williams, G. V.; Kramer, S. *Phys. Rev. B* **2000**, *62*, 4132.
(9) Mochiku, T.; Mihara, Y.; Hata, Y.; Kamisawa, S.; Furuyama, M.; Susuki, J.; Kadowaki, K.; Metoki, N.; Fujii, H.; Hirata, K. *J. Phys. Soc. Jpn.* **2002**, *71*, 790.
(10) Slater, P. R.; Greaves, C. *Physica C* **1991**, *180*, 299.

10.1021/cm034624q CCC: $25.00
Published on Web 11/19/2003

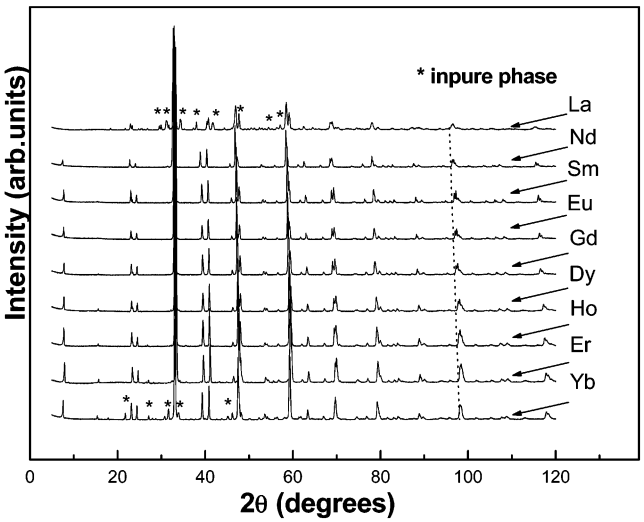

Figure 1. XRD patterns of $FeSr_2LnCu_2O_{7+\delta}$ (Ln = La, Nd, Sm, Eu, Gd, Dy, Ho, Er, and Yb).

To find other ferromagnetic superconductors, in this paper we report a series of new compounds $FeSr_2LnCu_2O_{7+\delta}$ for Ln = La, Nd, Sm, Eu, Gd, Dy, Ho, Er, and Yb. We determine the crystal structure of these compounds by means of X-ray diffraction and Mössbauer spectroscopy. Magnetization and resistance measurements are also carried out.

2. Experimental Section

Polycrystalline $FeSr_2LnCu_2O_{7+\delta}$ samples were prepared by a solid-state reaction. The starting materials are high purity (>99.9%) La_2O_3, Nd_2O_3, Sm_2O_3, Eu_2O_3, Gd_2O_3, Dy_2O_3, Ho_2O_3, Er_2O_3, Yb_2O_3, Fe_2O_3, $SrCO_3$, and CuO. The raw powder was preheated separately at 200 °C for 5 h and weighed according to the stoichiometric compositions, calcined at 900 °C for 12 h in air, and then ground and pressed into pellets. The pellets were sintered at 980 °C for 48 h in air. Finally, the samples were quenched to room temperature in the air. In addition, for as-synthesized sample $FeSr_2GdCu_2O_{7+\delta}$, two samples were prepared with the as-synthesized sample: one after annealing at 600 °C for 12 h under flowing O_2 [O_2-annealed] and the other after annealing at 600 °C for 12 h under flowing N_2 [N_2-annealed]. A subsequent furnace cooling was allowed for both samples in O_2 and N_2 atmosphere, correspondingly. The particular temperature of 600 °C was chosen because at this temperature region the kinetics of oxygen intercalation in the 1:2:3 structures are maximized. Finally, we should also mention that annealing of the as-synthesized sample $FeSr_2GdCu_2O_{7+\delta}$ at 900 °C in flowing N_2 destroyed this phase.

X-ray powder diffraction (XRD) data used for structural analysis were collected on a Rigaku D/max 2500 diffractometer with Cu Kα radiation (50 kV × 250 mA) and a graphite monochromator. A step-scan mode was employed with a step width of $2\theta = 0.02°$ and a sampling time of 1 s. The XRD patterns showed that the compounds are single phase except for some minor impure phase for Ln = La and Yb (see Figure 1). The XRD data were analyzed by the Rietveld refinement program DBWS-9411.[11,12]

The oxygen contents of the samples were chemically determined by the iodometric titration.[13,14] The concentration of sodium thiosulfate titrant was standardized against 99.999% pure CuO powder. About 200 mg of the powder sample was put into 20 mL of 10% hydrochloric acid. Starch indicator with the concentration of 2% was added immediately before the titration end point. The whole process of the titration was performed under strong stirring with an electromagnetic stirrer, and completed within 20 min for one sample.

A ^{57}Fe Mössbauer spectrum of the as-synthesized and O_2-annealed compound $FeSr_2GdCu_2O_{7+\delta}$ were recorded at room temperature in transmission geometry.

The temperature dependence of magnetization curves in a field of 1 kOe in the range of 5−300 K was measured by means of a superconducting quantum interference device (SQUID) magnetometer. Electrical resistance was measured by the standard four-probe method from 300 down to 5 K in zero field.

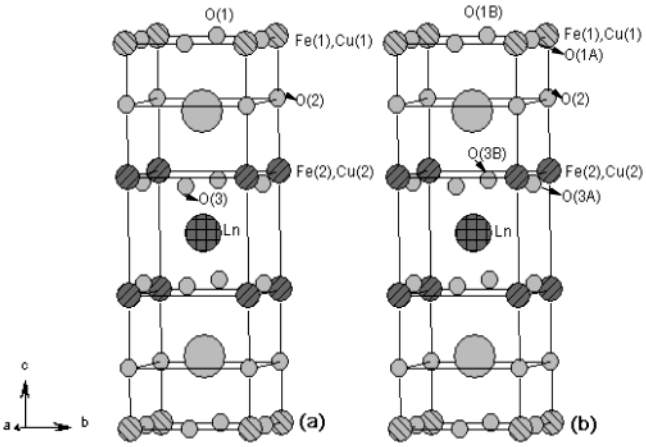

Figure 2. (a) Tetragonal $FeSr_2LnCu_2O_{7+\delta}$ structure; (b) orthorhombic $FeSr_2LnCu_2O_{7+\delta}$ structure.

Table 1. Structure Model Based on the Space Group *P4/mmm* and Based on the Space Group *Pmmm*

atom	site	*x*	*y*	*z*	Occ.
		P4/mmm			
Sr	2h	1/2	1/2	z	1
Ln	1d	1/2	1/2	1/2	1
Fe(1),Cu(1)	1a	0	0	0	1
Fe(2),Cu(2)	2g	0	0	z	1
O(1)	2f	0	1/2	0	N
O(2)	2g	0	0	z	1
O(3)	4i	0	1/2	z	1
		Pmmm			
Sr	2t	1/2	1/2	z	1
Ln	1h	1/2	1/2	1/2	1
Fe(1),Cu(1)	1a	0	0	0	1
Fe(2),Cu(2)	2q	0	0	z	1
O(2)	2q	0	0	z	1
O(3A)	2s	1/2	0	z	1
O(3B)	2r	0	1/2	z	1
O(1B)	1e	0	1/2	0	N
O(1A)	1b	1/2	0	0	N

3. Results and Discussion

3.1 Structure Refinement. The XRD data of the compounds $FeSr_2LnCu_2O_{7+\delta}$ (Ln = La, Nd, Sm, Eu, Gd, Dy, Ho, Er, and Yb) for the 2θ region between 5° and 120° were used for the refinement. It could be completely indexed on the basis of both the tetragonal space group *P4/mmm* (based on the $CuBa_2GdCu_2O_{6.06}$,[15] see Figure 2(a) and Table 1) and the orthorhombic *Pmmm* (based on the $CuBa_2GdCu_2O_{6.99}$,[15] see Figure 2(b) and Table 1) of the Fe1212 structure type. In only $FeSr_2$-

(11) Rietveld, H. M. *Acta Crystallogr.* **1967**, *229*, 151.
(12) Young, R. Y.; Sakthirel, A.; Moss, T. S.; Paiva-Santos, C. O. *J. Appl. Crystallogr.* **1995**, *28*, 336.
(13) Chen, X. L.; Liang, J. K.; Wang, C.; Yuan, W. X.; Xing, X. R.; Qiao, Z. Y. *J. Alloys Compd.* **1994**, *209*, 65.
(14) Harris, D. C.; Hewston, T. A. *J. Solid State Chem.* **1987**, *69*, 182.
(15) Guillaume, M.; Allenspach, P.; Henggeler, W.; Mesot, J.; Roessli, B.; Staub, U.; Fischer, P.; Trounov, V. *J. Phys. Condens. Matter* **1994**, *6*, 7963.

Table 2. Final Results of the Rietveld Refinements for the $FeSr_2LnCu_2O_{7+\delta}$ (Ln = La, Nd, Sm, Eu, and Gd) Compounds in Space Group *P4/mmm*[a]

	La	Nd	Sm	Eu	Gd
oxygen content	7.28(5)	7.38(3)	7.40(1)	7.36(3)	7.34(12)
radius for Ln^{3+}(Å)	1.160	1.109	1.079	1.066	1.053
R_{wp}	13.04%	11.28%	9.86%	10.20%	11.14%
R_p	10.59%	7.45%	6.68%	7.02%	7.43%
R_{exp}	2.53%	2.97%	2.70%	2.83%	2.55%
a (Å)	3.8789(1)	3.8633(2)	3.8559(1)	3.8502(3)	3.8457(1)
b (Å)	3.8789(1)	3.8633(2)	3.8559(1)	3.8502(3)	3.8457(1)
c/3 (Å)	3.8308(8)	3.8289(1)	3.8091(1)	3.8028(1)	3.7965(4)
V (Å^3)	172.913	171.439	169.902	169.117	168.442
z_{sr}	0.1600(12)	0.1861(5)	0.1854(12)	0.1835(2)	0.1829(3)
B_{Sr} (Å^2)	1.6	1.6	1.6	1.6	1.6
B_{Ln}(Å^2)	0.7	0.7	0.7	0.7	0.7
$B_{Cu(1)}$ (Å^2)	0.5	0.5	0.5	0.5	0.5
$z_{Cu(2)}$	0.3392(15)	0.3427(8)	0.3448(4)	0.3466(11)	0.3471(4)
$B_{Cu(2)}$ (Å^2)	1.0	1.0	1.0	1.0	1.0
$N_{O(1)}$	0.64	0.69	0.70	0.68	0.67
$B_{O(1)}$ (Å^2)	3.5	3.5	3.5	3.5	3.5
$z_{O(2)}$	0.1580(10)	0.1585(4)	0.1590(8)	0.1601(1)	0.1602(7)
$B_{O(2)}$ (Å^2)	2.4	2.4	2.4	2.4	2.4
$z_{O(3)}$	0.3578(12)	0.3681(6)	0.3685(4)	0.3706(3)	0.3704(6)
$B_{O(3)}$ (Å^2)	0.9	0.9	0.9	0.9	0.9

[a] The atomic isotropic temperature factors were kept fixed at the values obtained by Takashi Mochiku et al. (see ref 9).

Table 3. Final Results of the Rietveld Refinements for the $FeSr_2LnCu_2O_{7+\delta}$ (Ln = Dy, Ho, Er, and Yb) Compounds in Space Group *Pmmm*[a]

	Dy	Ho	Er	Yb
oxygen content	7.36(1)	7.40(4)	7.36(0)	7.42(7)
radius for Ln^{3+}(Å)	1.027	1.015	1.004	0.985
R_{wp}	9.61%	8.87%	10.26%	12.57%
R_p	6.48%	5.85%	6.58%	8.43%
R_{exp}	2.61%	2.25%	2.24%	2.43%
a (Å)	3.8274(2)	3.8213(1)	3.8159(1)	3.8115(1)
b (Å)	3.8329(1)	3.8274(1)	3.8229(1)	3.8180(1)
c/3 (Å)	3.7884(2)	3.7894(1)	3.7914(1)	3.7952(2)
V (Å^3)	166.728	166.267	165.926	165.685
z_{sr}	0.1818(6)	0.1804(5)	0.1806(2)	0.1836(3)
B_{Sr} (Å^2)	0.2	0.2	0.2	0.2
B_{Ln} (Å^2)	0.2	0.2	0.2	0.2
$B_{Cu(1)}$ (Å^2)	0.3	0.3	0.3	0.3
$z_{Cu(2)}$	0.3483(1)	0.3497(3)	0.3501(4)	0.3516(5)
$B_{Cu(2)}$ (Å^2)	0.2	0.2	0.2	0.2
$z_{O(2)}$	0.1610(11)	0.1604(8)	0.1608(12)	0.1606(11)
$B_{O(2)}$ (Å^2)	0.3	0.3	0.3	0.3
$z_{O(3A)}$	0.3781(4)	0.3743(8)	0.3790(13)	0.3807(11)
$B_{O(3A)}$ (Å^2)	0.5	0.5	0.5	0.5
$z_{O(3B)}$	0.3754(5)	0.3728(10)	0.3780(3)	0.3809(3)
$B_{O(3B)}$ (Å^2)	0.5	0.5	0.5	0.5
$N_{O(1B)}$	0.44(3)	0.44(1)	0.40(2)	0.48(2)
$B_{O(1B)}$ (Å^2)	2.0	2.0	2.0	2.0
$N_{O(1A)}$	0.92(3)	0.96(3)	0.96(4)	0.94(2)
$B_{O(1A)}$ (Å^2)	2.0	2.0	2.0	2.0

[a] The atomic isotropic temperature factors were kept fixed at the values obtained by M. Guillaume et al. (see ref 15).

$LaCu_2O_{7+\delta}$ and $FeSr_2YbCu_2O_{7+\delta}$ some minor impurity phase appeared (about 4% and 3%, respectively) which could be indentified as $SrCuO_2$ and Sr_2CuO_3. This is the main reason for the poor fits in these cases (see Tables 2 and 3). In our initial refinements, two variants of refinement were carried out: adopting both the orthorhombic and the tetragonal space group for all samples. In the final refinement, the following sites were assigned to Fe and Cu: 1a site for Cu(1) and Fe(1), and 2g (in space group *P4/mmm*) or 2q site (in space group *Pmmm*) for Cu(2) and Fe(2). The structural parameters, except for the occupation factors (Occ), are the same for the Cu (1) and Fe (1) sites and also for the Cu (2) and Fe (2) sites. In these compounds, the occupation factors of the Cu(1), Fe(1), Cu(2), and Fe(2) sites have the linear constraints: $Occ_{Cu(1)} = 2Occ_{Fe(2)}$; $Occ_{Fe(1)} = 1-2Occ_{Fe(2)}$; and $Occ_{Cu(2)} = 1-Occ_{Fe(2)}$. We cannot determine accurately the occupancy of Fe in 1a and 2g sites by the X-ray powder diffraction data because the atomic scattering factor of Cu and Fe are very close. The occupancy of Fe in 1a and 2g sites is obtained from Mössbauer spectra (see section 3.2). The oxygen contents of the samples were derived from the result of the iodometric titration and kept fixed in our refinements. The Rietveld refinement of the X-ray diffraction data shows that samples exhibit a transition from the tetragonal to the orthorhombic structure with the decrease of trivalent Ln ions radius. We got better R factors for the samples $FeSr_2LnCu_2O_{7+\delta}$ (Ln = La, Nd, Sm, Eu, and Gd) refined by space group *P4/mmm* and for the samples $FeSr_2LnCu_2O_{7+\delta}$ (Ln = Dy, Ho, Er, and Yb) refined by space group *Pmmm*. Table 2 shows the final results of the

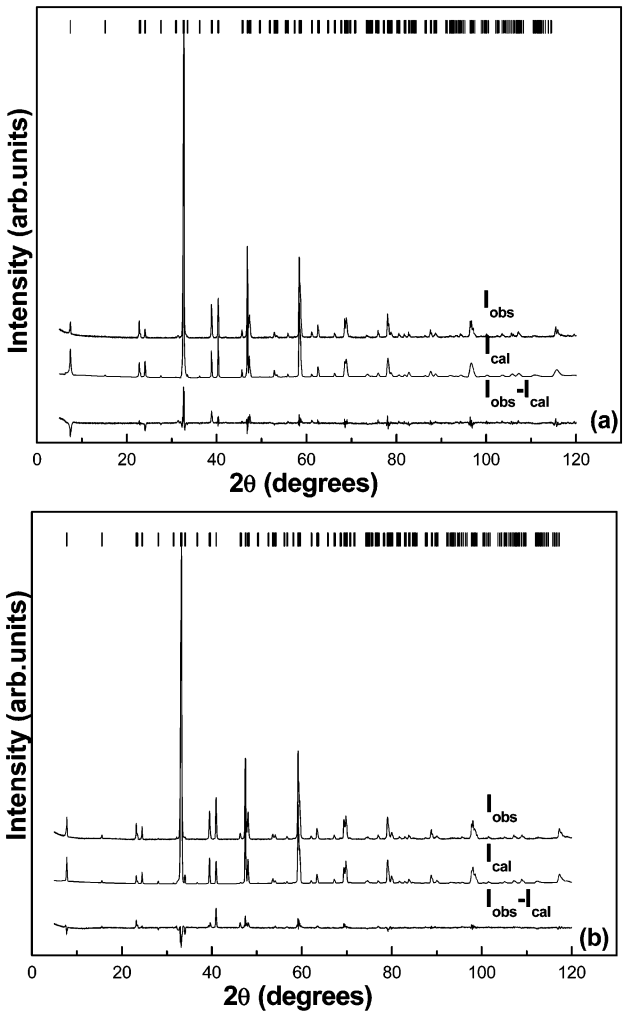

Figure 3. Observed, calculated, and difference XRD patterns of (a) $FeSr_2NdCu_2O_{7.38}$ (space group *P*4/*mmm*); and (b) $FeSr_2DyCu_2O_{7.36}$ (space group *Pmmm*).

Rietveld refinements for the $FeSr_2LnCu_2O_{7+\delta}$ (Ln = La, Nd, Sm, Eu, Gd) compounds in space group *P*4/*mmm*, and Table 3 shows final results of the Rietveld refinements for the $FeSr_2LnCu_2O_{7+\delta}$ (Ln = Dy, Ho, Er, Yb) compounds in space group *Pmmm*. The oxygen contents determined by iodometric titration for all samples are also given in Tables 2 and 3. Compounds $FeSr_2LnCu_2O_{7+\delta}$ (Ln = Dy, Ho, Er, and Yb) refined in space group *Pmmm* achieve better R factors than those refined in *P*4/*mmm*. Finally, the atomic isotropic temperature factors for the tetragonal system compounds were kept fixed at the values obtained from neutron powder diffraction studies in $FeSr_2YCu_2O_{7.36}$.[9] And atomic isotropic temperature factors for orthorhombic system compounds were also kept fixed at the values derived from neutron powder diffraction study in $HoBa_2Cu_3O_{7.02}$.[15] Typical best fits for tetragonal $FeSr_2NdCu_2O_{7.38}$ and for orthorhombic $FeSr_2DyCu_2O_{7.36}$ are shown in Figure 3(a) and (b), respectively. The vertical bars at the top indicate the expected Bragg reflection positions, and the lowest curve is the difference between observed and calculated patterns. Rykov et al.[16] reported that when substituting Fe for Ga in compound $HoSr_2Cu_2GaO_7$, compound $HoSr_2Cu_2FeO_7$ belongs to a tetragonal system with lattice parameters $a = 3.8232$ Å and $c = 11.384$ Å. This result is consistent with our sample $FeSr_2HoCu_2O_{7.4}$ refined by space group *P*4/*mmm* in principle. But we get smaller R factors for this sample refined by space group *Pmmm* ($R_{wp} = 8.87\%$) than that refined by space group *P*4/*mmm* ($R_{wp} = 11.23\%$). Thus, we think our experiment result is reasonable.

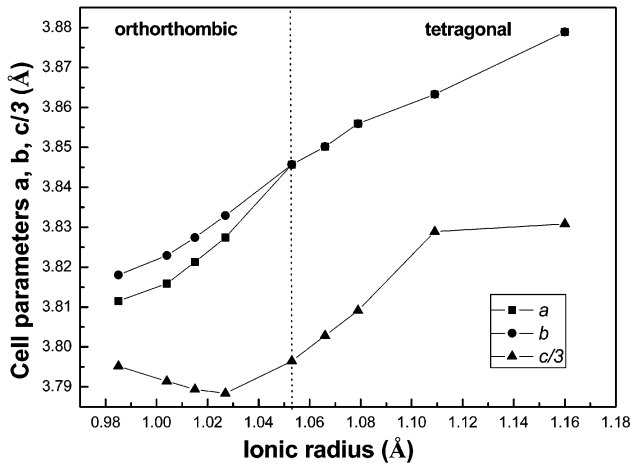

Figure 4. Lattice parameters *a*, *b*, and *c*/*3* of $FeSr_2Cu_2LnO_{7+\delta}$ versus radius of trivalent Ln ions.

Figure 4 shows the lattice parameters *a*, *b*, and *c*/*3* of the compounds $FeSr_2LnCu_2O_{7+\delta}$ versus radius of trivalent Ln ions.[17] It is easy to see that the tetragonal-to-orthorhombic structural transition corresponds to the composition at Ln = Gd. The lattice parameters *a* and *b* decrease with the decreasing of the radius of trivalent Ln ions. But an interesting point is that the lattice parameter *c* of tetragonal compounds of $FeSr_2LnCu_2O_{7+\delta}$ (Ln = La, Nd, Sm, Eu, and Gd) decreases with decreasing of the radius of trivalent Ln ions, whereas the lattice parameter *c* of orthorhombic compounds $FeSr_2LnCu_2O_{7+\delta}$ (Ln = Dy, Ho, Er, and Yb) slightly increases with decreasing of the radius of trivalent Ln ions. The lattice parameter *c* of compound $FeSr_2LaCu_2O_{7+\delta}$ deviates for monotonic relationship. This is possibly due to the fact that the content of oxygen in the $FeSr_2LaCu_2O_{7+\delta}$ ($\delta = 0.28$) is different from those in other members of $FeSr_2LnCu_2O_{7+\delta}$ ($\delta \approx 0.36-0.4$). The unit cell volume (Figure 5) clearly shows the expected lanthanide contraction behavior, i.e., it exhibits a linear relationship in principle when plotted versus the ionic radius for trivalent rare-earth ions in tetragonal and orthorhombic systems, respectively. The lattice parameter *c* of all compounds $FeSr_2LnCu_2O_{7+\delta}$ is smaller than that of the $LnBa_2Cu_3O_7$ compound, probably due to the fact that Sr has a smaller ionic radius than Ba. The insensitivity to the lattice parameter *a* of the Sr substitution indicates that the value of *a* is controlled by the Cu(1)−O layers. In the series of compounds $FeSr_2LnCu_2O_{7+\delta}$ the structural transition from orthorhombic to tetragonal (see Figure 4) with the increasing of Ln^{3+} ionic radius and a jump of unit cell volume and lattice parameter *c* takes place in compound Ln = Gd. This phenomenon is possibly related to the electron structure of rare earth elements. The tetragonal system is formed with the number of 4f

(16) Rykov, A.; Caignaert, V.; Raveau, B. *J. Solid State Chem.* **1994**, *109*, 295.

(17) Shannon, R. D. *Acta Crystallogr. A* **1976**, *32*, 751.

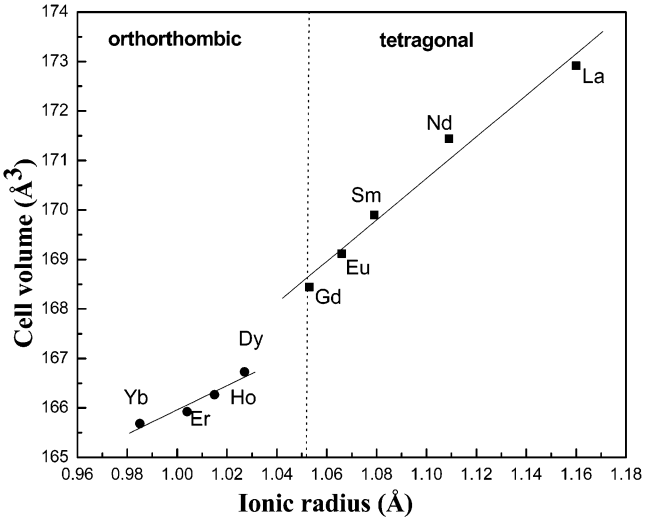

Figure 5. Unit cell volume $FeSr_2LnCu_2O_{7+\delta}$ versus radius of trivalent Ln ions.

Table 4. Selected Bond Distances (Å) and Numbers of Equivalent Bonds, *N*, in the Compounds $FeSr_2LnCu_2O_{7+\delta}$ (Ln = La, Nd, Sm, Eu, and Gd)

	La	Nd	Sm	Eu	Gd	*N*
Sr−O(1)	2.673	2.881	2.865	2.844	2.835	4
Sr−O(2)	2.743	2.750	2.743	2.736	2.732	4
Sr−O(3)	2.988	2.846	2.845	2.874	2.874	4
Ln-O(3)	2.536	2.455	2.444	2.426	2.424	8
Fe(1),Cu(1)−O(1)	1.939	1.932	1.928	1.925	1.923	4
Fe(1),Cu(1)−O(2)	1.816	1.821	1.817	1.817	1.825	2
Fe(2),Cu(2)−O(2)	2.082	2.116	2.123	2.128	2.129	1
Fe(2),Cu(2)−O(3)	1.951	1.954	1.947	1.944	1.941	4
Fe(2),Cu(2)−Fe(2),Cu(2)	3.696	3.614	3.547	3.500	3.483	1

Table 5. Selected Bond Distances (Å) and Coordination Numbers, *N*, in the Compounds $FeSr_2LnCu_2O_{7+\delta}$ (Ln = Dy, Ho, Er, and Yb)

	Dy	Ho	Er	Yb	*N*
Sr−O(2)	2.719	2.714	2.710	2.710	4
Sr−O(3A)	2.941	2.919	2.959	2.946	2
Sr−O(3B)	2.916	2.904	2.946	2.946	2
Sr−O(1A)	2.818	2.805	2.802	2.831	2
Sr−O(1B)	2.816	2.803	2.804	2.829	2
Ln-O(3A)	2.365	2.388	2.355	2.343	4
Ln-O(3B)	2.381	2.396	2.361	2.339	4
Fe(1),Cu(1)−O(2)	1.830	1.823	1.827	1.825	2
Fe(1),Cu(1)−O(1A)	1.914	1.911	1.911	1.906	2
Fe(1),Cu(1)−O(1B)	1.916	1.914	1.908	1.909	2
Fe(2),Cu(2)−O(2)	2.133	2.151	2.155	2.176	1
Fe(2),Cu(2)−O(3A)	1.943	1.931	1.936	1.935	2
Fe(2),Cu(2)−O(3B)	1.940	1.932	1.937	1.938	2
Fe(2),Cu(2)−Fe(2),Cu(2)	3.439	3.420	3.410	3.384	1

electrons ≤ 7, whereas the orthorhombic system is formed with the number of 4f electrons > 7.

We now proceed to discuss in detail some relevant interionic distances. Tables 4 and 5 list the selected interatomic distances and coordination numbers of the tetragonal and orthorhombic $FeSr_2LnCu_2O_{7+\delta}$ compounds, respectively. Figure 6 shows the separations of the CuO_2 plane for the $FeSr_2LnCu_2O_{7+\delta}$ compounds, i.e., the distances Fe(2),Cu(2)−Fe(2),Cu(2), which are particularly sensitive to the lanthanide contraction, since the rare-earth ions are sandwiched between the CuO_2 planes. In fact, the Fe(2),Cu(2)−Fe(2),Cu(2) distances are found to contract with the decreasing of the radius of trivalent Ln ions. To examine the reliability of the

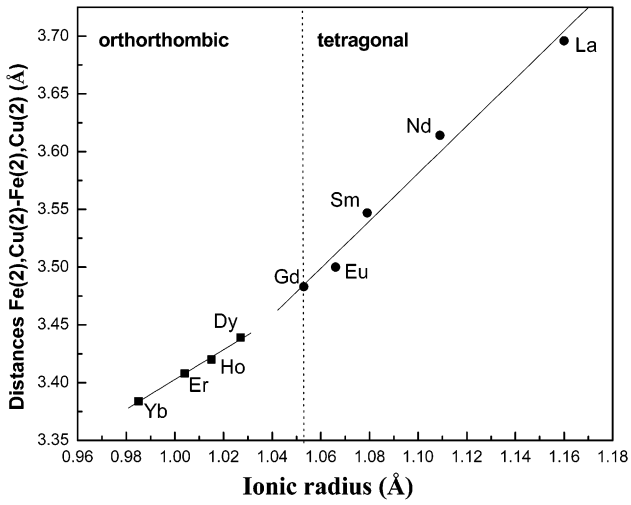

Figure 6. Distances Fe(2),Cu(2)−Fe(2),Cu(2) of $FeSr_2Cu_2LnO_{7+\delta}$ versus radius of trivalent Ln ions.

Table 6. Bond Valence Sums of the Sr, Ln Atom, Fe Atom at the 1a Site, and the Cu Atom at the 2g or 2q Site

	La	Nd	Sm	Eu	Gd	Dy	Ho	Er	Yb
V_{Sr}	1.69	1.63	1.67	1.69	1.67	1.57	1.70	1.68	1.62
V_{Ln}	2.99	3.10	3.07	3.09	3.09	2.93	2.97	2.97	2.90
V_{Fe}	3.29	3.41	3.48	3.40	3.39	3.39	3.47	3.45	3.53
V_{Cu}	2.25	2.21	2.24	2.25	2.27	2.26	2.30	2.27	2.26

determined structure, we used the bond valence model to estimate the valence of the ions shown in Table 6 by Brown relationship between bond valence and interatomic distance.[18] The valences of the Sr, Ln atom and Cu atom on the 2g or 2q site, Fe atom on the 1a site, V_{Sr}, V_{Ln}, V_{Cu}, and V_{Fe} are estimated using the bond distances listed in Table 4 and Table 5. From the result of our estimated V_{Sr}, V_{Ln}, and V_{Cu} (see Table 6), one can see that they are close to the chemical valence of Sr, Ln, and Cu atoms, respectively, and both Fe^{4+} and Fe^{3+} coexist in $FeSr_2LnCu_2O_{7+\delta}$ system. So we conclude that the structure determined by our Rietveld refinement is reliable.

The Rietveld refinements were also carried out for the samples $FeSr_2GdCu_2O_{7+\delta}$ after annealing in flowing N_2 [N_2-annealed] and in flowing O_2 [O_2-annealed]. In Figure 7 the Rietveld profile refinements of N_2-annealed and O_2-annealed samples are shown in the region 38° ≤ 2θ ≤ 50°. The refined parameters are listed in Table 7. In Table 7 the reported oxygen contents of the samples were chemically determined by the iodometric titration. We can see that the annealing atmosphere seems to affect considerably the oxygen contents of the system.

The sensitivity of the oxygen content to the annealing atmosphere is also manifested in the variation of certain structural parameters. The *z* coordinate of the Sr atom exhibits a large variation from $z = 0.1786$ [O_2-annealed] to $z = 0.1944$ [N_2-annealed], and it is in close similarity to what has been reported for the 1:2:3 superconductors as the oxygen content decreases. This Sr movement toward the Cu(2)−O plane in the N_2-annealed samples causes the inversion of the relative intensities of the (014) and (113) reflections (Figure 7) as well as the considerable increase in the intensity of the (114)

(18) Brown, I. D.; Altermatt, D. *Acta Crystallogr. B* **1985**, *41*, 244.

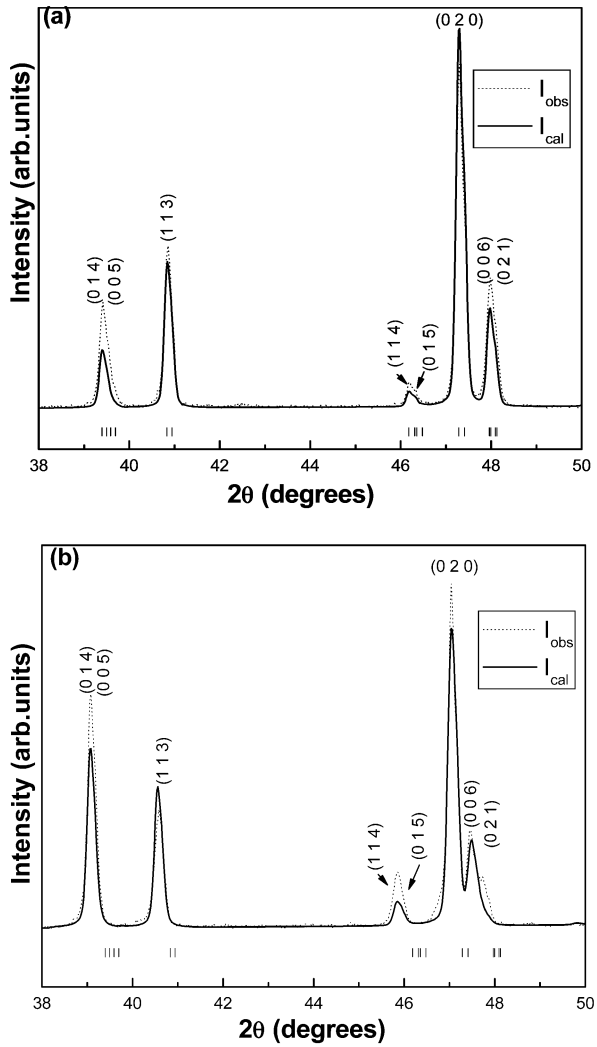

Figure 7. Rietveld refinement patterns for $FeSr_2LnCu_2O_{7+\delta}$ (a) O_2-annealed and (b) N_2-annealed, in the region $38° \leq 2\theta \leq 50°$.

reflection which is clearly shown in the N_2-annealed sample. In addition, the unit cell volume shows a considerable increase as the oxygen decreases due to decreasing of average valence and increasing of ionic radius of cations. The length of the *c* axis (which can be taken as a measure of the oxygen content in the 1:2:3 superconductor) presents exactly the same variation with the oxygen content as for 1:2:3, i.e., the higher the oxygen content, the shorter the *c* axis.[19−21]

3.2 Mössbauer Spectra Study. Because the X-ray scattering factors of Fe and Cu are very close, it is not possible to accurately determine the distribution of Fe among 1a and 2g sites in *P*4/*mmm* or 1a and 2q sites in *Pmmm* of Fe1212 structure compounds. Mössbauer spectroscopy has been proven a powerful tool in the determination of the oxidation state of the Fe atoms as well as their environment (i.e., crystallographic site in the structure). Although it is now apparent that the details of the Mössbauer spectra depend on the heat

Table 7. Final Results of the Rietveld Refinements for the $FeSr_2GdCu_2O_{7+\delta}$ after Annealing in Flowing O_2 and in Flowing N_2 with Space Group *P*4/*mmm*[a]

	O_2-annealed	N_2-annealed
oxygen content	7.38(5)	7.16(3)
R_{wp}	10.71%	11.23%
R_p	7.02%	7.80%
R_{exp}	3.03%	2.95%
a (Å)	3.8422(2)	3.8578(1)
b (Å)	3.8422(2)	3.8578(1)
c (Å)	11.3731(3)	11.4731(3)
V (Å^3)	167.900	170.750
z_{sr}	0.1786(11)	0.1944(2)
B_{Sr} (Å^2)	1.4	1.3
B_{Ln}(Å^2)	0.5	0.5
$B_{Cu(1)}$ (Å^2)	1.9	0.3
$z_{Cu(2)}$	0.3400(1)	0.3470(4)
$B_{Cu(2)}$ (Å^2)	0.4	0.9
$N_{O(1)}$	0.69(5)	0.58(3)
$B_{O(1)}$ (Å^2)	2.2	2.5
$z_{O(2)}$	0.1597(1)	0.1577(4)
$B_{O(2)}$ (Å^2)	1.9	2.1
$z_{O(3)}$	0.3739(2)	0.3737(10)
$B_{O(3)}$ (Å^2)	0.7	0.9

[a] The atomic isotropic temperature factors were kept fixed at the values obtained by Takashi MochikU et al. (see ref 9) from neutron powder diffraction studies in $FeSr_2YCu_2O_{6+\delta}$ (N_2-annealed and O_2-annealed samples).

treatment and oxygen stoichiometry of the samples as well as on the amount of iron, a considerable amount of experimental evidence appears to be at least qualitatively well-established. In particular, there are clearly at least four iron sites which are immediately identifiable by their hyperfine parameters [isomer shift (IS), quadrupole splitting (2ϵ), and saturation hyperfine field (H)]. Lines and Eibschutz[22] label these sites *A* (IS = 0.28 mm/s, 2ϵ = 0.5 mm/s), *B* (IS = 0.00 mm/s, 2ϵ = 1.19 mm/s), *C* (IS = −0.15 mm/s, 2ϵ = 1.61 mm/s), and *D* (IS = 0.04 mm/s, 2ϵ = 1.94 mm/s) in order of increasing room-temperature quadrupole splitting, and it is this labeling we are going to use below. In the 300 K Mössbauer spectrum of $FeSr_2GdCu_2O_{7.34}$ [as-synthesized], three paramagnetic quadrupole doublets are show in Figure 8(a). These are analyzed with three components *A*, *C*, and *D* (according to the labeling of Lines and Eibschutz[20]). The intensity of C covers 38.7-(40)% of total intensity and the isomer shift of −0.038-(20) mm/s relative to *a*-Fe indicates either high-spin Fe^{4+} or low-spin Fe^{3+} and its quadrupole splitting is 0.688(33) mm/s. Component *D* covers 28.0(34)% and has a typical Fe^{3+} isomer shift of 0.174(21) mm/s, and its quadrupole splitting is 1.615(48) mm/s. The last component *A* covers 33.3(3) %. Its isomer shift of 0.278(23) mm/s is typical of high-spin Fe^{3+}, the quadrupole splitting is 0.612(40) mm/s. Comparison with the result of Mössbauer analysis for $FeSr_2YCu_2O_y$[23] and $YSr_2Cu_2FeO_y$[24] compounds can lead us to the conclusion that components *C* and *D* come from iron located at the 1a site. Thus, the total Fe occupancy at the 1a site amounts to 66.7(9) % and an occupancy of 16.7(3) % at the 2g site.

Figure 8(b) shows the Mössbauer spectrum of $FeSr_2GdCu_2O_{7.38}$ [O_2-annealed] at RT; these are also analyzed

(19) Kallias, G.; Niarchos, D. *Supercond. Sci. Technol.* **1992**, *5*, 56.
(20) Cava, R. J.; Hewat, A. H.; Heweat, E. A.; Batlogg, B.; Marezio, M.; Rabe, K. M.; Krajewski, J. J.; Peck, W. F., Jr.; Rupp, L. W. *Physica C* **1990**, *165*, 419.
(21) Jorgensen, J. D.; Veal, B. W.; Paulikas, A. P.; Nowicki, L. J.; Crabtree, G. W.; Claus, H.; Kwok, W. K. *Phys. Rev. B* **1990**, *41*, 1863.
(22) Lines, M. E.; Eibschutz, M. *Physica C* **1990**, *166*, 235.
(23) Awana, V. P. S.; et al. *Physica B* **2002**, *312−313*, 62.
(24) Pissas, M.; Kallias, G.; Simopoulos, A.; Niarchos, D.; Kostikas, A. *Phys. Rev. B* **1992**, *46*, 14119.

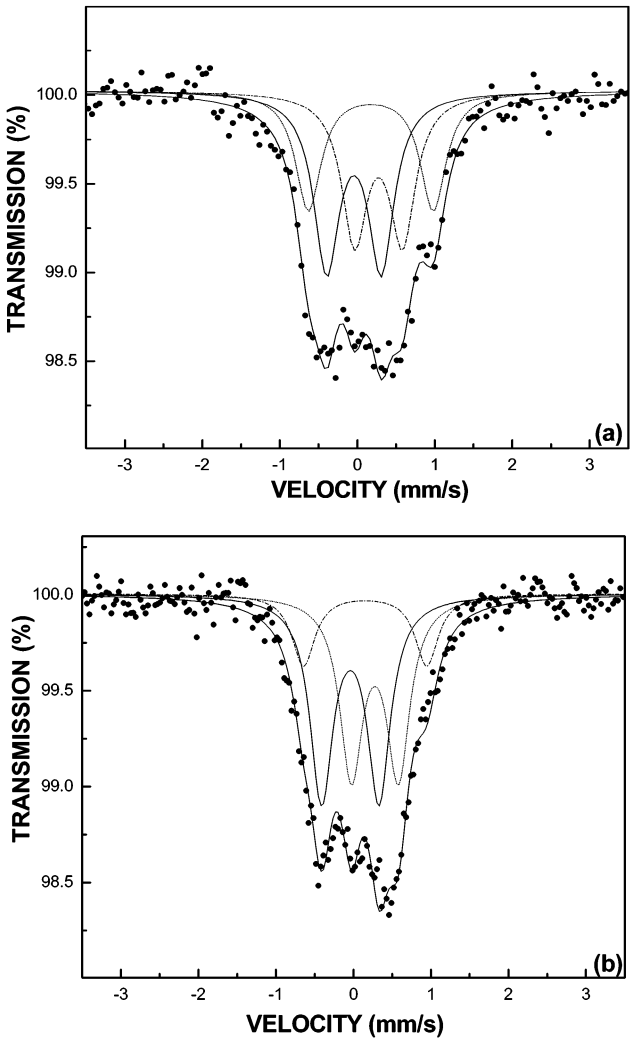

Figure 8. Fitting of the ^{57}Fe Mössbauer spectrum recorded at room temperature for the $FeSr_2GdCu_2O_{7+\delta}$ (a) as-synthesized and (b) O_2-annealed.

with three components *A*, *C*, and *D*. The intensity of *C* covers 44.7(36)% of total intensity, and the isomer shift of −0.042(13) mm/s relative to *a*-Fe indicates either high-spin Fe^{4+} or low-spin Fe^{3+}. Its quadrupole splitting is 0.742(24) mm/s. Component *D* covers 15.9(31)% and has a typical Fe^{3+} isomer shift of 0.150(30) mm/s, and its quadrupole splitting is 1.590(73) mm/s. The last component *A* covers 39.4(27)%. Its isomer shift of 0.275(16) mm/s is typical of high-spin Fe^{3+}, the quadrupole splitting is 0.607(29) mm/s. Thus, the total Fe occupancy at the Cu(1) site amounts to 60.6% and 19.7% at the C(2) site. Comparison with the result of Mössbauer analysis for $FeSr_2GdCu_2O_{7.34}$ [as-synthesized], we can see that the Fe atom has a preference for the 1a site and a small number of Fe atoms (6%) migrate from the 1a site to the 2g site after annealing at 600 °C in flowing O_2.

3.3 Magnetization and Electrical Resistance. To clarify the magnetic properties of this system, magnetization measurements were also performed from 5 K to room temperature for the as-synthesized and O_2-annealed samples (Ln = Nd, Gd, and Er). The observed magnetic susceptibilities for Ln = Nd, Gd, and Er shown in Figure 9a, b, and c, respectively, indicate that χ changes with temperature in a Curie-type manner. The

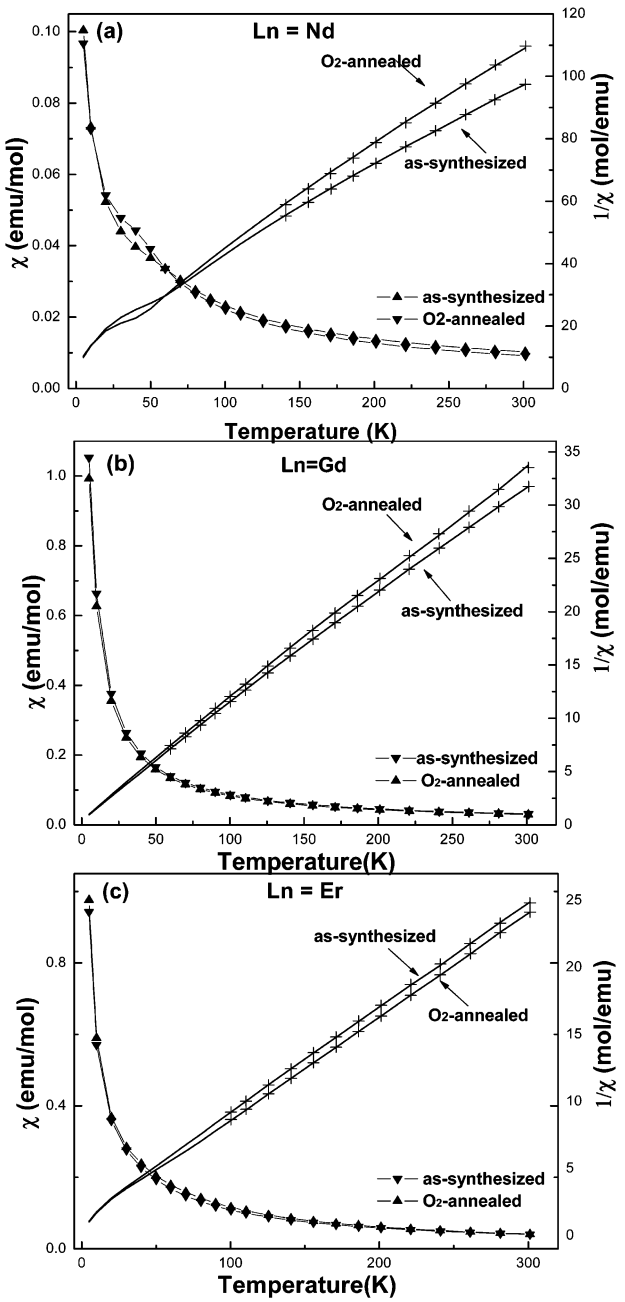

Figure 9. Magnetic susceptibility in a field of 1 kOe as a function of temperature for several members of the $FeSr_2LnCu_2O_{7+\delta}$ series: (a) Ln = Nd, (b) Ln = Gd, and (c) Ln = Er.

data can be fitted to a Curie−Weiss law of general formula

$$\chi_g = \chi_0 + C_g/(T - \Theta)$$

where χ_0 and Θ are the temperature-independent susceptibility and Weiss constant, respectively, and C_g is the Curie constant given by the relation

$$C_g = N\mu_{eff}^2\mu_B^2/3k$$

where N is the number of ions that carry a magnetic moment per unit volume, μ_{eff} is the effective number of magneton per ion, μ_B is the Bohr magneton, and k is the Boltzman constant. The parameters χ_0, C_g, and Θ were determined by a least-squares fit for the temperature range 60−300 K. The values of the magnetic

Table 8. Parameters Obtained from a Fit to a Curie−Weiss Law; Shown Are the Weiss Constant (Θ), the Temperature-Independent Susceptibility (χ_0), the Effective Magnetic Moment (μ_{eff}) Derived from the Curie Constant (C), and the Temperature Interval over Which the Fit Was Determined

Ln		C	Θ	χ_0 (10^{-4} emu/mol)	μ_{eff} (obs)	μ_{eff} (cal)	fitting interval
Nd	as-synthesized	4.01	−89.5	1.1	5.66	7.06	150−300 K
	O_2-annealed	3.74	−68.6	2.2	5.46	7.01	150−300 K
Gd	as-synthesized	10.35	−27.5	1.4	9.096	9.99	60−300 K
	O_2-annealed	9.57	−18.9	0.5	8.749	9.96	60−300 K
Er	as-synthesized	12.88	−41.5	1.6	10.15	11.34	100−300 K
	O_2-annealed	12.95	−7.58	1.2	10.18	11.32	100−300 K

moments and the Weiss constant deduced from the fits are reported in Table 8. The plot of $(\chi - \chi_0)^{-1}$ vs T (Figure 9) produces straight lines as expected for a Curie-type behavior for Ln = Gd compound. Compounds with Ln = Nd and Er show a deviation from the Curie−Weiss law below 60 K as shown in Figure 9a and 9c. This anomaly at low temperature may arise from crystal electric field (CEF) splitting of the ground state J-multiplet or a small amount of antiferromagnetic impurity phase.

The experimental effective magnetic moments extracted from the C values for as-synthesized and O_2-annealed samples $FeSr_2LnCu_2O_{7+\delta}$ (Ln = Nd, Gd, and Er) are also listed in Table 8. In this system, there are four ions per unit cell that carry a magnetic moment, two copper atoms having $S = {}^1/_2$, a rare earth atom, and one iron ion. From our Mössbauer spectra study for the Ln = Gd compound, the iron ion consists of 38.7% of the Fe in the $S = 2$ state (high spin Fe^{4+}), 28% of the Fe in typical Fe^{3+} state ($S = {}^5/_2$), and 33.3% of Fe in high-spin Fe^{3+} state ($S = {}^5/_2$). For the O_2-annealed sample, the iron ion consists of 44.7% of the Fe in the $S = 2$ state (high spin Fe^{4+}), 15.9% of the Fe in typical Fe^{3+} state ($S = {}^5/_2$), and 39.4% of Fe in high-spin Fe^{3+} state ($S = {}^5/_2$). The theoretic μ_{eff} contributed by Fe ions listed in Table 8 for Ln = Nd and Er compounds are calculated using the oxidative state for Fe ions in $FeSr_2GdCu_2O_{7+\delta}$.

From Table 8, one can see that the value of experimental effective magnetic moment for the as-synthesized sample (Ln = Nd and Gd) is larger than that of the O_2-annealed sample. This behavior may result from the changes of oxidative state for Fe ions in this system. Mössbauer spectra study for the Ln = Gd compound shows that the concentration of high-spin Fe^{4+}($S = 2$) increases and that of Fe^{3+} ($S = {}^5/_2$) decreases after annealing at 600 °C in flowing O_2, so the effective magnetic moment contributed by Fe ions should decrease correspondingly. Because the effective magnetic moment of two copper ions and one rare earth ion remains unchanged, the decrease of effective magnetic moment for Fe ions will lead to a decrease of effective magnetic moment for the sample. Compound Ln = Nd has the same crystal structural type as the Ln = Gd compound, so the decrease of effective magnetic moment may derive from same mechanism.

Focusing on the Ln = Er compound, the experimental effective moment increases after annealing at 600 °C in flowing O_2. This behavior may reflect the structural transition for Ln = Er compound which differed from the one of compounds Ln = Gd and Nd; further experiments are needed to clarify this issue.

Electrical resistance measurements were carried out in zero field from 5 to 300 K. Figure 10a and b show the conductivity (σ) in zero field as a function of the temperature for tetragonal system samples $FeSr_2LnCu_2O_{7+\delta}$ (Ln = Nd, Sm, and Gd) and orthorhombic system compound $FeSr_2LnCu_2O_{7+\delta}$ (Ln = Dy, Ho, and Er), respectively. It is obvious that the compounds $FeSr_2LnCu_2O_{7+\delta}$ (Ln = Nd, Sm, Gd, Dy, Ho, and Er) exhibit a semiconductor-like behavior. This result is consistent with the sample with an overdroped charge (i.e., by the Fe and Co atom) on the CuO_2 in $YBa_2Cu_3O_{6+\delta}$ system.

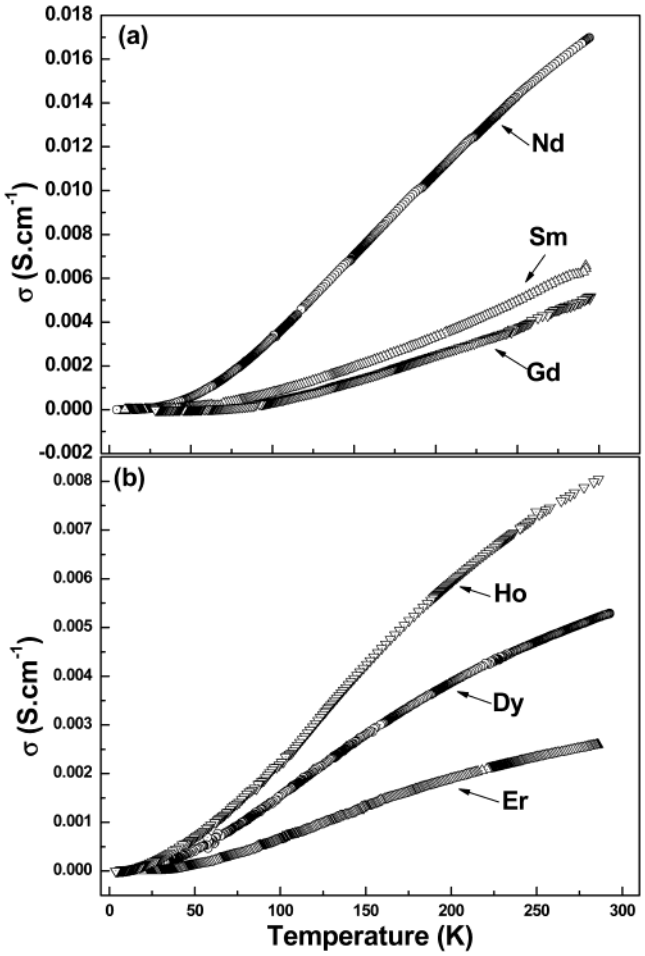

Figure 10. Electrical conductivity of $FeSr_2LnCu_2O_{7+\delta}$ as a function of temperature: (a) tetragonal $FeSr_2LnCu_2O_{7+\delta}$ systems (Ln = Nd, Sm, and Gd), and (b) orthorhombic $FeSr_2LnCu_2O_{7+\delta}$ system (Ln = Dy, Ho, and Er).

To understand the origin of the semiconductor behavior of these samples and the effects on conductive behavior due to the crystal structural transition, we have analyzed σ (T) in some detail. We found that a single activated dependence of σ on T cannot account for the entire range of conductivity data of the series Fe-1212 compounds. The low-temperature ($T \leq 150$ K) transport tends to be dominated by a very low density of localized states introduced by impurities and non-

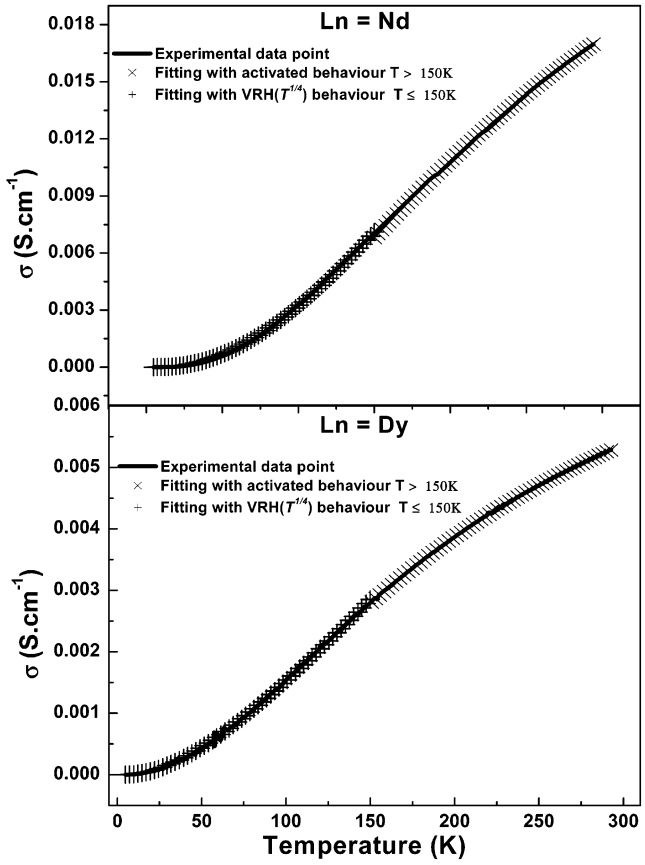

Figure 11. Best fit to electric conductivity for compound $FeSr_2NdCu_2O_{7.38}$ with the space group *P*4/*mmm* and $FeSr_2ErCu_2O_{7.36}$ with the space group *Pmmm*.

stoichiometry within the band gap region of the stoichiometry compound, whereas the high-temperature (T > 150 K) behavior is contributed by the thermally activated charge carriers across the band gap. In view of these two contributions to the conductivity, we model the conductivity dependence on temperature in the low-temperature range as

$$\sigma(T) = \sigma_0 \exp[-(T_0/T)^{1/4}]$$

The term in the above expression accounts for variable-range hopping (VRH) within the localized low density of states in the midgap region, where σ_0 is constant. In the region of 150 K < $T \leq$ 300 K, we model it as

$$\sigma(T) = \sigma_0 \exp[-Eg/2KT]$$

This equation represents the activated behavior. Typical best fits for tetragonal $FeSr_2NdCu_2O_{7.38}$ and for orthorhombic $FeSr_2DyCu_2O_{7.36}$ are shown in Figure 11a and b, respectively. The activation energy obtained by a good fit in the high-temperature versus radius of trivalent rare earth ions is shown in Figure 12. From Figure 12, one can see the activation energy exhibits a linear increase with the contraction of ionic radius for trivalent rare-earth ions in tetragonal compounds $FeSr_2LnCu_2O_{7+\delta}$ (Ln = Nd, Sm, and Gd) and orthorhombic compounds

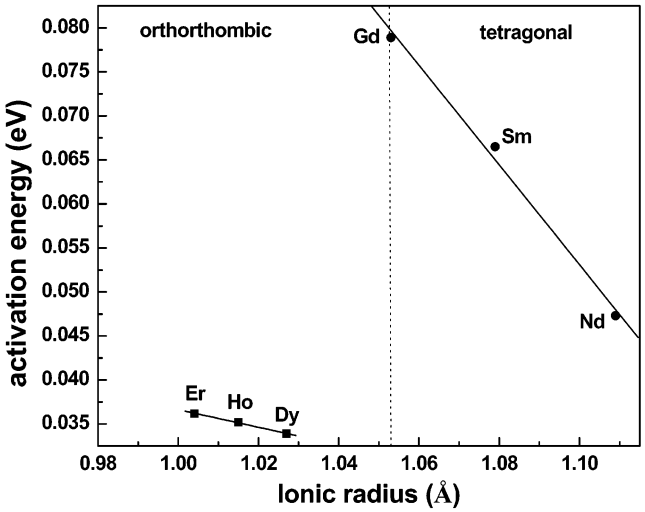

Figure 12. Activation energy for the series of compounds $FeSr_2LnCu_2O_{7+\delta}$ (Ln = Nd, Sm, Gd, Dy, Ho, and Er) as a function of radius of trivalent Ln ions.

$FeSr_2LnCu_2O_{7+\delta}$ (Ln = Dy, Ho, and Er), and the activation energy of tetragonal compounds is obviously larger than that of orthorhombic compounds. The value of activation energy for the whole series of compounds $FeSr_2LnCu_2O_{7+\delta}$ goes through a dramatic jumping at the point Ln = Gd at which structural phase transition takes place as mentioned in Section 3.1.

Electric properties analysis shows the band gap for tetragonal compounds is wider than that of orthorhombic compounds in this Fe-1212 system; and in compounds with the same crystal structures, the ionic radius of rare-earth ions plays an important role in determining the value of their activation energy.

4. Conclusion

We provide for the first time a consistent set of structural data for carefully prepared new Fe1212 compounds. It is apparent that the replacement of a CuO_4 structural unit by an FeO_6 unit is able to stabilize these nonexisting phase $LnSr_2Cu_3O_7$. The Rietveld refinements of the X-ray diffraction data show that samples exhibit a transition from the tetragonal to the orthorhombic systems from light rare earths to heavy rare earths. Magnetization and electric properties of this series of compounds clearly reflect the structural transition. To find a new method to enhance the degree of ordering between Fe and Cu atoms may improve the conductivity of this series of compounds, even reaching superconductivity. Work addressing this problem is in progress.

Acknowledgment. This work is supported by the State Key Project of Fundamental Research (NKBRSF-G19990466) and the National Natural Science Foundation of China (50272083). We thank J. R. Chen and S. Y. Fan for the XRD and magnetic measurements.

CM034624Q